Energy 115 (2016) 1216–1233

Contents lists available at ScienceDirect

Energy

journal homepage: www.elsevier.com/locate/energy

# Reducing the environmental impact of hydraulic fracturing through design optimisation of positive displacement pumps

Aleksandar Josifovic [a, *], Jennifer J. Roberts [b], Jonathan Corney [a], Bruce Davies [a], Zoe K. Shipton [b]

[a] Design, Manufacture and Engineering Management, 75 Montrose Street, University of Strathclyde, Glasgow, G1 1XJ, United Kingdom
[b] Civil & Environmental Engineering, 75 Montrose Street, University of Strathclyde, Glasgow, G1 1XJ, United Kingdom

ARTICLE INFO

*Article history:*
Received 4 November 2014
Received in revised form
26 August 2016
Accepted 4 September 2016

*Keywords:*
Hydraulic fracturing equipment
System optimisation
Environmental impact
Multivariable analysis
Positive displacement pump
Energy efficiency

ABSTRACT

The current approach to hydraulic fracturing requires large amounts of industrial hardware to be transported, installed and operated in temporary locations. A significant proportion of this equipment is comprised of the fleet of pumps required to provide the high pressures and flows necessary for well stimulation. Studies have shown that over 90% of the emissions of $CO_2$ and other pollutants that occur during a hydraulic fracturing operation are associated with these pumps. Pollution and transport concerns are of paramount importance for the emerging hydraulic fracturing industry in Europe, and so it is timely to consider these factors when assessing the design of high pressure pumps for the European resources.

This paper gives an overview of the industrial plant required to carry out a hydraulic fracturing operation. This is followed by an analysis of the pump's design space that could result in improved pump efficiency. We find that reducing the plunger diameter and running the pump at higher speeds can increase the overall pump efficiency by up to 4.6%. Such changes to the pump's parameters would results in several environmental benefits beyond the obvious economic gains of lower fuel consumption. The paper concludes with a case study that quantifies these benefits.

© 2016 The Authors. Published by Elsevier Ltd. This is an open access article under the CC BY license (http://creativecommons.org/licenses/by/4.0/).

## 1. Introduction

The technology of hydraulic fracturing was first demonstrated in the 1950s [1] and has subsequently been used to enhance the permeability of a range of geological resources, including potable water, geothermal heat, and conventional onshore and offshore hydrocarbon resources [2]. In the past decade combination of horizontal drilling technologies and hydraulic fracturing has transformed energy markets by enabling the economic extraction of unconventional gas resources, including coal bed methane and more notably shale gas.

The International Energy Agency (IEA) [3] has estimated that, by 2035, gas demand will have increased by 50% on 2011 levels. Such growth would impact on the global energy mix and see gas overtake coal as the second largest energy source after oil. The same report also suggested that after 2020 unconventional gas extraction will account for 32% of the total gas production (currently this figure is estimated to be about 14%). If the figures suggested by the IEA report are to be realized, gas extraction from unconventional sources will have to double by 2020. Interest in unconventional sources of hydrocarbons has also been motivated by the desire to ensure the security of Europe's gas supply [4].

Although estimates suggest there are significant potential shale gas reserves in Europe (e.g. Britain [5], France and Poland [6]), exploration has been limited and to date no large scale extraction operations have commenced. This is largely because concerns about a range of environmental and social impacts have prevented the granting of legal licence for the process in a number of countries. While there are some potential subsurface risks (such as well integrity failure leading to groundwater pollution, or earth tremors from the hydraulic fracturing process), arguably, surface installations pose the greatest potential environmental and social risks [7]. These risks include surface water pollution, light and noise pollution, traffic, and air quality [8]. In the UK, for example, operators have been refused licences to carry out hydraulic fracturing operations because of concerns about the noise of the machinery [9], and road traffic [10]. Thus the potential environmental impacts must be minimised if shale gas extraction operations are to be

* Corresponding author.
*E-mail address:* aleksandar.josifovic@strath.ac.uk (A. Josifovic).

http://dx.doi.org/10.1016/j.energy.2016.09.016
0360-5442/© 2016 The Authors. Published by Elsevier Ltd. This is an open access article under the CC BY license (http://creativecommons.org/licenses/by/4.0/).

permitted in Europe.

There are also concerns about the climate change implications of unconventional gas extractions; from the direct and indirect greenhouse gas (GHG) emissions from the shale gas extraction process itself, and more generally from the continued exploitation of fossil fuel reserves and the subsequent increase of the global gas market. GHG emissions are a key element of industrial impact, so it is essential that the onshore oil and gas sector develops scenarios for $CO_2$ reduction, similar to those adopted in other industries [11]. The methodologies for doing this are well understood. For example, the development of a computational model for estimating $CO_2$ emission from oil and gas extraction was discussed in Gavenas et al. (2015), which allowed the main sources of GHG emissions to be identified, managed and mitigated [12]. Since it is forecast that gas will remain a significant fuel in the future, it is important to minimise the emissions intensity of the shale gas extraction process in order for the resource to be developed in-line with current carbon emissions reductions targets. Life cycle assessments (LCAs) are an important tool that can inform the relative carbon intensity of different energy choices, and so identify means of reducing overall emissions. There is some uncertainty around the magnitude of GHG emissions from shale gas extraction and currently the majority of reported shale gas LCAs have been performed using North American data and practices. Issues such as differences in assumptions and scope of the LCAs can make their results difficult to compare, and estimates of lifecycle emissions are evolving as new measurements become available and as commercial practices change in response to environmental regulation or technological advances. Furthermore, these LCAs must be adapted to the European context, which differ from North America in terms of the resource, environmental regulations, and social factors. A recent comparative meta-analysis of LCAs found that the median difference between electricity generated from unconventional and conventional gas in North America was 3% [13]. These results are similar to LCAs adapted for shale gas extraction in the EU [14]. Indeed, LCAs adapted for shale gas extraction in the UK [15] and Scotland [16] find that the carbon intensity of shale gas could be lower than imported conventional natural gas. These LCAs identify that besides fugitive leaks of methane during gas extraction and transport, which could be the greatest source of GHG emissions from shale gas, the majority of GHG emissions arise from activities during the preparation of the well pad and construction of the well, rather than during gas production [16]. To further reduce the carbon intensity of shale gas and the environmental footprint of the industry, operators should seek to minimise the area of the well pad, the amount of surface infrastructure, size and mass of the construction materials, distances that materials are transported, and the pad power requirements.

Local air quality, noise and traffic issues associated with hydraulic fracturing activity impact on communities local to shale gas developments, and concerns around these impacts are causing delays to planning applications in the UK and negatively affecting public acceptance of the industry [17]. The construction and operation of the surface facility requires significant truck movements and transport distances. For example in North America over 1000 truck round trips are required for a single hydraulic fracturing site [18]. Diesel fumes from trucks, drilling, frac-pump engines and emissions from gas processing equipment can significantly reduce the air quality around a hydraulic fracturing site; both for the workers, and local residents [19]. While some significant air quality issues in America are related to practices that would not be permitted in Europe due to environmental legislation (such as storage of flowback fluids in open ponds), the effect of diesel engines from trucks and pump engines will result in a decrease of local air quality as well as contributing to noise pollution. Recent work by Rodriguez et al. (2013) [19] measured fuel consumption and on site emissions for two hydraulic fracturing sites in North America, and found that the fracturing pumps contribute to 90% of total emissions on site. The pumping equipment may also generate the most significant noise on site during the lifetime of the shale gas operations, depending on the number of pumps in operation at any time [17].

In North America, the development of surface hardware has, to-date, largely been driven by the need for incremental responses to the need for hydraulic fracturing at higher pressures and greater depths. These requirements (high fluid pressure and transport of proppants into the well bore) place great demands on the mechanical structures of the pumps and therefore the pumps require frequent maintenance and have finite lives. However there is no reason why the site machinery deployed in the EU needs to be to the same specifications as in the North American sites. For example, an enhanced pump design could contribute to reducing the environmental footprint of the well construction and completion, and also of any re-fracturing during the lifetime of the shale gas well. Given the relative infancy of the shale gas industry in Europe, it is timely to consider opportunities for improved design of required hardware.

In this paper, we consider how site machinery, and pumps in particular, could be designed to meet both functional and environmental specifications. There is relatively little information available in published peer-reviewed literature about the practical ‘on site’ aspect of the equipment, energy and water requirements for the exploration of European shale gas reserves. Thus, we first provide an overview of the industrial plant required to carry out a hydraulic fracturing operation. We then consider the functional requirements (i.e. pressure and flow) of the equipment adapted to the European geologic context, before applying a parametric model to analyse the design space of a pump's reciprocating components and solve for both functional performance and efficiency. We present the changes to the pump design, and then discuss the associated benefits of these more efficient pumps in terms of the physical and environmental footprint of the pumping operations.

## 2. Methodology

The location of a well stimulation operation by means of hydraulic fracturing is commonly referred to as a “frac-site”. The frac-site consists of an array of pumps, engines, liquids, sand, pipework and wellbore hardware that can weigh over a thousand tonnes, involve 30–40 operators and cover an area of few thousand squared metres (the total area of a frac site is typically ~3000 $m^2$[14]). The mechanical pumps which create the pressures and flows required are central to the process.

The depth and therefore hardness of the rock formation being stimulated (i.e. fraced) have steadily increased since 1950s requiring larger pressures and flow rates. The pumping equipment has matched these increasing demands through incremental development of existing designs.

Although there are number of commercial pump suppliers there is remarkable uniformity in the mechanical design (e.g. plunger diameter, speed and stroke length). Rather than simply adopting the industry's default values this paper investigates the “design space” of several critical interacting parameters to identify an optimum solution. To do this the following methodology was adopted:

1. Establish the duty cycle of hydraulic fracturing hardware in the context of single and multi-stage fracs;
2. Identify the typical pressure and flow required to fracture low permeability rock at the required depths;

3. Detail all the elements of the mechanical systems used to generate the high pressure used during hydraulic fracturing;
4. Use a parametric mathematical model to quantify the behaviour of the pumps for any configuration;
5. Develop optimisation algorithm to explore possible efficiency improvements and identify best set of design parameters;
6. Use exemplar scenarios based on frac-site case study to compare power and performance requirements from current and next generation of pumps;
7. Quantify the environmental benefits that enhanced pump performance could offer for hydraulic fracturing operations;

The approach of modelling mechanical systems and then optimizing their parameters to improve performance has been employed in other process industries. For example Santa et al. (2015) employs this methodology for determining the most efficient choice of design parameter values for a heat pump [20].

The physical and performance characteristics of the optimised pump design are examined, with particular emphasis on pump efficiency. The potential impacts of more efficient pumps on the environmental and social impacts of hydraulic fracturing operations are then qualitatively assessed. We also propose opportunities for further improvements to high pressure pump design and operation. This approach will result in an improved pump design that is applicable to any hydraulic fracturing activities (in other words, not limited to shale gas extraction applications).

## 3. Process overview

This section gives an overview of the process of hydraulic fracturing. We initially detail a single "stage" of hydraulic fracturing and then discuss how the process is conducted across a number of stages covering the entire "pay zone" of the well (i.e. the gas-rich target rock). Typical values for the major process parameters (e.g. speed, pressure, flow and time) are presented for each step. These have been obtained from site visits and available literature (both commercial and academic), and the sources are identified in the text.

### 3.1. Single pumping stage

In order to hydraulically fracture a well, fluids (comprised mostly of water) are injected under high pressure to stress the rock until it cracks. Once hairline fractures have been formed they need to be held open for gas to flow out, otherwise rock will close due to the pressure exerted by the weight of the rock above (referred to as overburden pressure). To do this the fractures are propped open with sand (or other proppant), that is added to the frac-fluid [21]. Gas then flows from the rock into the well bore, via these propped fractures, once fluid pressure is reduced (usually by pumping). After a clean-up phase (e.g. pumping of the frac water from the well, clearing of site, removal of earth works, all of which may take up to 40 days [22]) the well is ready for production.

The hydraulic fracturing process can be illustrated concisely by referring to one of the performance monitoring graphs recorded in the control truck. On the right hand axis of Fig. 1 slurry (i.e. water flow rate) and proppant concentration (i.e. sand) volumes are plotted against time during a two and a half hour fracturing operation. On the left hand axis, pressure is plotted. Slurry rate in Fig. 1 refers to total flow (litres/min) of frac-fluid from the pump array. Proppant concentration refers to the percent of sand combined with the frac-fluid (slurry) [21].

The pressure plot in Fig. 1 reaches its peak (fracture initiation) early in the stage after which it reduces and is held roughly constant to ensure fracture propagation. Flow rate is also held constant from the moment the cracks are initiated to ensure correct fracture size (i.e. desired width, height and length). Proppant is introduced towards the middle of the cycle, and the particle size of the proppant is systematically varied during the hydraulic fracturing process, starting with larger and ending with finer grain size. The proppant concentration increases continually while the grain size is reduced, which is necessary to ensure created fissures are "propped" open with the grains supporting the overburden (i.e. the geological strata above the fracture).

### 3.2. Multi-stage hydraulic fracturing of the entire well

Wells are usually fractured in many places along the length of the well. The well is divided into a number of isolated sections, known as stages, which are then fractured individually. The number of sections (stages) depends on the length of the well, and can range from 1 up to 50 stages. Wells are fractured in stages to ensure fractures are created along the length of the bore (rather than only in the weakest area of the rock). To enable pressure containment

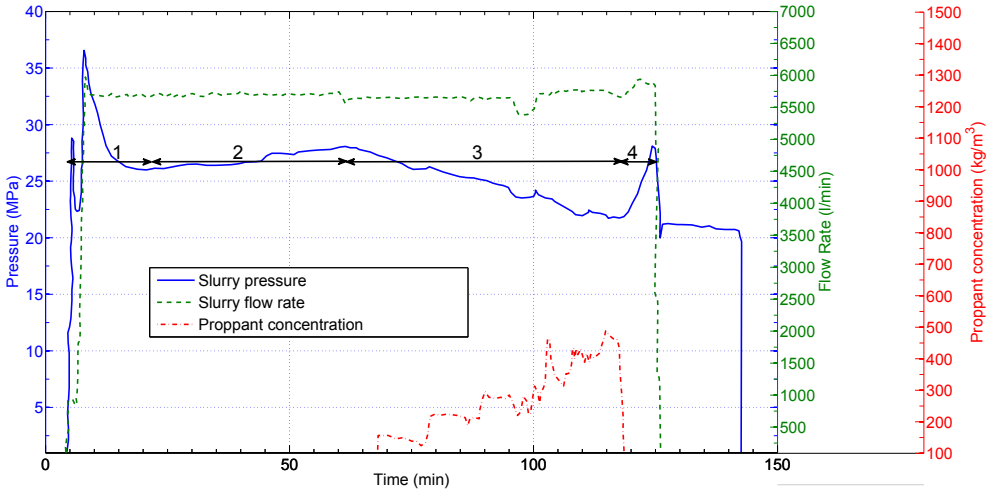


**Fig. 1.** The process of hydraulic fracturing can be characterized by the four combination of flow rate, pressure and proppant seen during a typical stage, (adapted from Ref. [51]). In phase 1 water is pumped at high pressure to initiate cracks in the well. Phase 2 delivers a high flow rate at a reduced pressure and in this phase formed cracks are enlarged and expanded. Proppant is introduced in phase 3 and finally, in phase 4, water is recirculated through the bore to displace proppant.

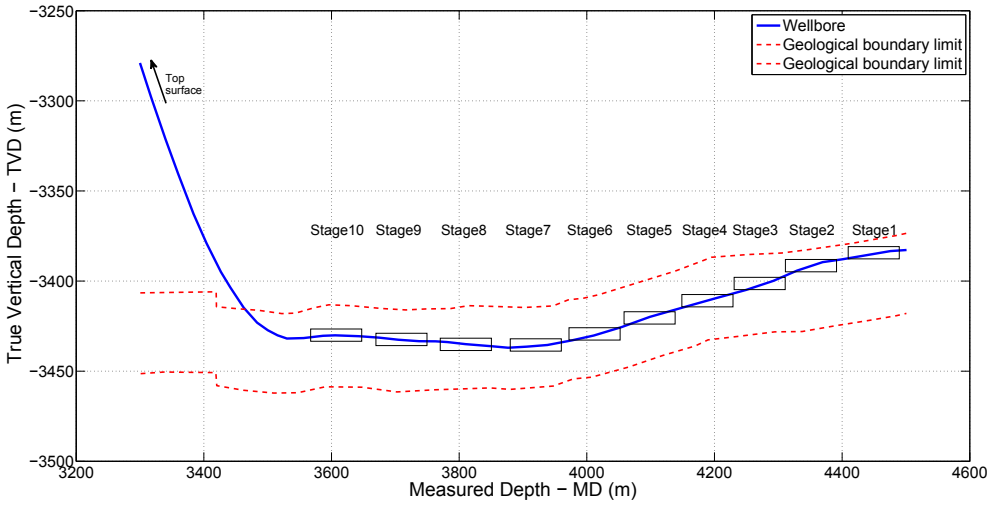


**Fig. 2.** The single stage stimulation process (shown in Fig. 1) is repeated along the length of the 'target zone' of a well in a sequence of operations that progresses from the end of the wellbore towards the surface. The figure is reproduced from original well data obtained from field trials [52].

within the desired area, a section of the well bore is closed off using packers [1]. Once that section is fractured and propped, the completed stage needs to be isolated to ensure that the next area is not affected by the previous stage [21].

Fig. 2 illustrates the process for an entire well where the boxed areas represent a single stage, described earlier in Fig. 1. Hydraulic fracturing starts from the far end of the well (i.e. right hand side of Fig. 2) and progressively moves to the heel of the wellbore, stage by stage. At the end of the hydraulic fracturing process (i.e. once all the stages have been fraced) all the internal parts (perforating gun and packers) are removed, and the frac-fluid first flows to surface (due to the high pressure in the well bore), and is then pumped from the well, allowing the free movement of gas along the length of the well to the surface.

## 4. Pressure and flow requirements

Any investigation into the mechanical redesign of hydraulic fracturing equipment must start by considering the necessary performance requirements. The following section provides estimates of the pressures and flow rates required to successfully stimulate a typical shale well.

### 4.1. Pressure

In order to establish the pressure needed to create a fracture the depth and the properties of the target rock formation must be determined. Although the structure of rock is very variable, the typical density, porosity and compressive stress values that define the material can be used to illustrate the order of magnitude of these parameters [22]. Even in the same basin, the depth of the prospective formations will vary significantly in terms of the upper and lower limits. For instance, in the Bowland Basin (UK), the upper limit of the formation range is around 1000m with the maximum thickness up to 4000m [23]. Furthermore, the rock properties (e.g. strength, density) will vary within the basin due to heterogeneities in the rock itself caused by natural variations in its formation and so the pressure required is not simply a function of depth.

Haimson and Fairhurst (1967) presented the following solution for fracture initiation and extension [24]. Assuming an isotropic, homogenous, linear elastic rock the stresses in the formation prior to any stimulation can be expressed as in Eq. (1). This expression supposes that a vertical wellbore radius, $r_w$, is drilled in the z-axis ($\sigma_z$ direction) and so defines the radial stress $\sigma_{rr}$, tangential stress $\sigma_{\theta\theta}$ and $\tau_{r\sigma}$ shear stress that exists around the wellbore. The radial

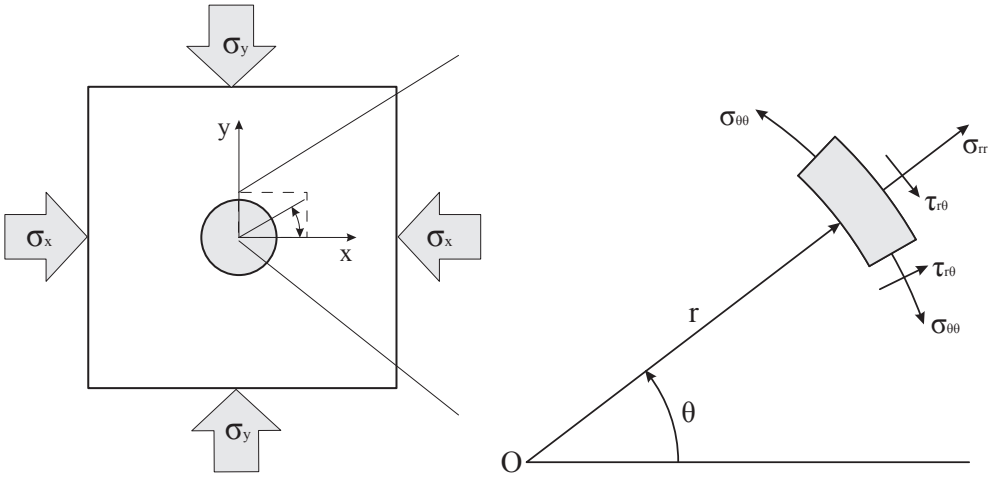


**Fig. 3.** The grey area in 3(left) represents a wellbore in a rock formation with surrounding stress fields associated with the overburden. In 3(right) all the stress vectors acting on an element of rock in the wall of the wellbore are illustrated.

distance is $r$ and the angle measured from the $\sigma_z$ direction is $\theta$, Fig. 3.

$$\sigma_{rr} = \frac{\sigma'_x + \sigma'_y}{2}\left(1 - \frac{r_w^2}{r^2}\right) + \frac{\sigma'_x - \sigma'_y}{2}\left(1 + 3\frac{r_w^4}{r^4} - 4\frac{r_w^2}{r^2}\right)\cos 2\,\theta$$
$$\sigma_{\theta\theta} = \frac{\sigma'_x + \sigma'_y}{2}\left(1 + \frac{r_w^2}{r^2}\right) - \frac{\sigma'_x - \sigma'_y}{2}\left(1 + 3\frac{r_w^4}{r^4}\right)\cos 2\,\theta$$
$$\tau_{r\sigma} = \frac{\sigma'_x - \sigma'_y}{2}\left(1 - 3\frac{r_w^4}{r^4} + 2\frac{r_w^2}{r^2}\right)\sin 2\,\theta \tag{1}$$

As a first approximation, let us assume $r = r_w$. Substituting this in Eq. (1) it can be concluded that $\sigma_{rr} = 0$ and $\tau_{r\sigma} = 0$. So the tangential stress in the rock, $\sigma_{\theta\theta}$ can be expressed using Eq. (2).

$$\sigma_{\theta\theta} = \sigma'_x + \sigma'_y - 2\left(\sigma'_x - \sigma'_y\right)\cos 2\,\theta \tag{2}$$

Thus, if $\sigma_z$ is acting in vertical direction the joint impact of both $\sigma_x$ and $\sigma_y$ stresses can be estimated. These stresses are present in the entire reservoir.

Fig. 4 shows the borehole deformation due to the acting stresses in X and Y directions. If $\sigma_x$ is assumed to be greater than $\sigma_y$ the direction of fracture propagation can be determined. A material element close to A-A′ are under tension while those close to B–B′ are under compression. Solid mechanics suggests that fracture initiates at a point, or points, of maximum tensile stress and that additional cracks will propagate in the direction of the maximum principle stress. Furthermore it is known that rock is almost an order of magnitude weaker in tension than in compression [25]. So it is clear that fracture will initiate in the A-A′ direction. Stress in A-A′ section, where $\theta = 0°$:

$$\sigma_{\theta\theta} = \sigma_x + \sigma_y - 2(\sigma_x - \sigma_y)(1)$$
$$\sigma_{\theta\theta} = 3\sigma_y - \sigma_x \tag{3}$$

Stress in B-B′ section, where $\theta$=90°:

$$\sigma_{\theta\theta} = \sigma_x + \sigma_y - 2(\sigma_x - \sigma_y)(-1)$$
$$\sigma_{\theta\theta} = 3\sigma_x - \sigma_y \tag{4}$$

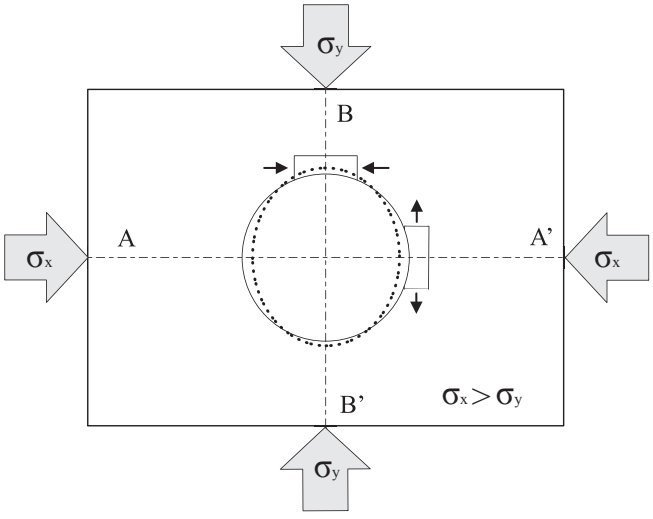


**Fig. 4.** Horizontal drilling typically creates asymmetric stress fields (a special case of Fig. 3(left)) Further analysis of stress fields shown in Fig. 3 considers stress distribution in XY direction in cases where $\sigma_x$ is greater than $\sigma_y$.

In order for a fracture to occur in the well, the maximum tensile stress induced around the wellbore must be greater than tensile strength of the formation. Indeed, if $\sigma_{\theta\theta} = 3\sigma_y - \sigma_x$ (the stress caused by the weight of the rock above the bore) exceeds the tensile strength of the formation then a fracture will occur in the process of drilling and hydraulic fracturing may not be necessary. However, if $\sigma_{\theta\theta}$ is not sufficient, fluid pressure must be applied to induce additional tensile stress in the wellbore. Stresses generated by internal fluid pressure can be estimated by applying Eq. (5). Pressure differential inside the wellbore ($\Delta p$) is the difference between the bottom-hole pressure ($p_w$) and the reservoir pressure ($p_r$).

$$\sigma_{rr} = (p_w - p_r)\frac{r_w^2}{r^2} = \Delta p\frac{r_w^2}{r^2}$$
$$\sigma_{\theta\theta} = -(p_w - p_r)\frac{r_w^2}{r^2} = -\Delta p\frac{r_w^2}{r^2} \tag{5}$$
$$\tau_{r\theta} = 0$$

So if tensile strength of the formation is considered it can be concluded that fracturing will occur whenever $\sigma_{\theta\theta}$ is equal to the tensile strength of the rock (T).

The effect of pore pressure ($p_r$) also needs to be accounted for when estimating fracture pressure. In 1923, Terzaghi introduced the concept of effective stress stating that the weight of the overburden is carried by the rock material (i.e. grains) and the pore pressure (the pressure of the fluid in the pore spaces between the rock grains). To refine this concept in 1941, Biot introduced a poroelastic constant, $\beta$, that describes the efficiency of fluid pressure [26]. The poroelastic constant $\beta$ can be obtained experimentally.

Eq. (1) can now be developed to include additional factors reflecting fluid pressure, Eq. (5), tensile strength of the rock ($T$) and Terzaghi/Biot stress distribution ($\beta p_r$). Finally, the breakdown pressure required to cause formation failure ($p_b$) can be expressed by Eq. (6).

Breakdown pressure ($p_b$) is the first phase of hydraulic fracturing. Once formation breakdown occurs, the overall pressure is generally reduced by 20–30%, as shown in Fig. 1. This phenomenon was explained by Haimson et al. [24] and Hubbert et al. [25] who also identifies the basic driving factors for fracture initiation during hydraulic fracturing.

$$p_b = 3\sigma_{Hmin} - \sigma_{Hmax} + T - \beta p_r \tag{6}$$

Having established the driving factors for the overall stress state, the most influential factors can be examined and discussed further. From Eq. (6) it is apparent that all the variables show linear correlation. However, $\sigma_{Hmin}$, (due to the multiplication factor 3) has the highest impact. The least principal horizontal stress $\sigma_{Hmin}$ is a direct result of the overburden stress and the Poisson's ratio of the material ($\upsilon$) determines how much vertical stress will be transmitted in the horizontal direction. Rocks with a high Poisson's ratio will have higher horizontal stress. Taking into account both the overburden carried by the rock grain and the overburden carried by the pore pressure ($\beta p_r$) the total horizontal stress equation can be expressed by Eq. (7).

$$\sigma_{Hmin} = \left(\frac{\upsilon}{1-\upsilon}\right)(\sigma_V - \beta p_r) + \beta p_r \tag{7}$$

Furthermore, Eq. (7) states that horizontal stress ($\sigma_{Hmin}$) is affected by vertical stresses of the overlying formation ($\sigma_V$) and pore pressure ($\beta p_r$) in the horizontal direction.

Poisson's ratio ($\upsilon$), poroelastic constant ($\beta$) and pore pressure ($p_r$) can all be derived by experimental analysis of the core samples [27]. Vertical stress ($\sigma_V$) is naturally affected by the height of the

overburden layer ($H$) and the average density ($\rho$) of the overlying strata Eq. (8).

$$\sigma_V = \rho H \tag{8}$$

$$22.62\frac{kPa}{m} \leq \sigma_V \leq 24.88\frac{kPa}{m} \tag{9}$$

A logging tool could be used to measure formation density of the individual layers in the overburden. However, due to the well depth and time involved it is more common to use an average pressure factor gradient as expressed in Eq. (9).

It can be concluded that depth is driving factor in determining the actual requirements of the well. In the case study (Section 8) sets of data are evaluated using these theoretical equations.

### 4.2. Volume

Having established the theoretical pressure needed to fracture the rock, the second pumping parameter, fluid volume, can now be investigated. There is no single property of shale rock that is able to accurately describe the volume of water required to hydraulically fracture each individual well. Due to geological differences in the properties of the rock, structural and the relative location of the shale prospective layers, predictions need to be adjusted appropriately. There is currently little publically available information about the properties of shale in Europe, and so North American shale data must be used to estimate the properties of the European equivalent shale. According to the API (American Petroleum Institute) guidelines, the magnitude of the liquid volume required to successfully hydraulically fracture well is somewhere between 9 million and 18 million litres [28], other papers report similar volumes [29].

The frac-fluid volume requirement can be divided into two quantities. First, the amount of water needed to fill all the hoses, pipelines and well casing up to the target zone (i.e. stage to be fractured). Second, the water absorbed in the cracked rock during the hydraulic fracturing. This approach requires both quantitative and qualitative assessment of the actual water requirement depending on the changes in the well properties (i.e. depth and shale rock characteristics). To calculate the volume required to fill the pipe work and bore on site it is necessary to examine all the lines leading from the water storage units on site to the shale reservoir rock (well depths are rarely shallower than 1000 m). Because surface leads and lines are measured in tens of metres (at least two orders of magnitude smaller than the well depth) the following discussion focuses only on estimating casing volume.

The outer wall of the bore is formed by casing strings run in sequence. Bigger diameter pipes are used at the start and as the well length progresses the casing diameter becomes smaller. The internal wall of the bore is created by a uniform production casing throughout the entire well. Since diameter is consistent from the surface to the end we can calculate the total volume (V) based on Eq. (10). Measured depth (MD) is the true well length from the surface to the end of the well, Fig. 2. The pipe's internal diameter is denoted by D.

$$V = \frac{D^2\pi}{4}MD \tag{10}$$

To evaluate the second volume of the water needed during hydraulic fracturing it is necessary to examine actual field data. Field data was collected from three different hydraulic fracturing operations in structurally different basins during April 2013. In each case the operational time of the hydraulic fracture for a single stage was between 60 and 210 min. A number of flow rates were recorded during operations but for brevity this paper will present only one stage per well (Table 1). It can be seen that the average volume flow rate is between 6,000 and 10,000 l/min. The volume of fluid needed to fill the casing, Eq. (10) would typically be only measure in tens of thousands of litres in total (e.g. 20,000 l) in other words only a fraction of the overall fluid requirements.

## 5. Machinery - size and volume

Machinery used throughout hydraulic fracturing can be divided into four categories:

- Transport equipment (i.e. trucks),
- Fluid servicing equipment (i.e blenders and mixers),
- Pipeline equipment (i.e. manifold trailer),
- Pressure pumping equipment (i.e. pump, diesel engine and transmission).

### 5.1. Transporting equipment

The entire process of hydraulic fracturing is designed to be portable because it will be active and present on site for only a few weeks [21]. On process completion the equipment is disassembled and transported to the next location. The time spent on site is dependent on the length of the well bore, number of wells, number of stages and the geology of the site.

Pumps, blender and pipe manifold are all mounted on trailers. Similarly, water, chemicals and sand are transported in separate containers. Hydraulic fracturing is just one of many procedures used to prepare a well for production.

The size and weight of the individual units (i.e frac-trailer assemblies) is in many instances the key design constraint, i.e. the component size and weight is limited by the truck specifications. In North America the maximum truck load limits are different from state to state. Consequently equipment manufactures try to design lighter and therefore universally usable components.

### 5.2. Fluid servicing equipment

There are multiple units on site that provide the various fluid services (i.e. to store, prepare, and separate the frac-fluids) shown of the right hand side of Fig. 6.

- Storage tanks - All the consumables are transported to the frac-site in plastic or steel containers depending on their chemical property. Additives commonly added to water are used to

**Table 1**
Experimental flow rate data during hydraulic fracturing [40].

| Well no. | Time (min) | Flow rate (l/min) | Average rate (l/min) | Total volume (l) |
|---|---|---|---|---|
| Well 1 | 57 | 1,908–8 904 | 6,698 | 381,759 |
| Well 2 | 97 | 1,590–7 950 | 6,376 | 618,510 |
| Well 3 | 210 | 1,590–16 224 | 13,144 | 2,472,100 |

enhance viscosity so that proppant is suspended in the fluid, decrease viscosity to clean up the bore, chemical breakers to release the sand from the slurry mixture and biocides to eliminate any bacteria from the water [30].

- Blender - This unit is used to mix all the ingredients into one consistent fluid commonly referred to as “slurry”. Depending on the desired effect downhole this fluid may be more or less (so called “slick” water) viscous than water. Proppant is transported into the blender's tub using augers, while chemicals and water use separate lines to supply the tub. Once the slurry mixture has been mixed, centrifugal pumps transfer the fluid to a common pipeline which feeds all the pumps.

### 5.3. Pipeline - manifold trailer

The intakes and outlets of all the pumps used to create the necessary pressures and flows are connected to the manifold trailer, Fig. 5. There are two separate circuits for low and high pressure in the manifold trailer.

The low pressure line of the manifold trailer transports fluid from the blender to the suction side of the positive displacement (PD) pumps. Depending on the configuration of the manifold trailer different numbers of inlet and outlet ports can be present. The line leading from blender to PD pumps is also known as the low pressure line. Pressure coming from the blender rarely exceeds 10 bar, therefore ports on this side of the manifold trailer in most instances are simple butterfly valves.

The high pressure line of the manifold trailer connects fluid coming from the discharge side of the PD pumps towards the wellhead. The high pressure line is positioned underneath the low pressure line. A hydraulic fracturing sites may have as many as 20 independent PD pumps with each pump capable of creating pressures up to 1000 bar (15,000 psi) [1]. Since significant fluid energy is being transmitted around the site special procedures are used to ensure safe operation. Constraining rings are incorporated in the manifold trailer and restraining ropes are used to tie down all the pipework leading fluid from the discharge side of the pump to the manifold trailer.

### 5.4. Pressure pumping equipment

Once slurry is mixed in the blender unit, fluid flows via a manifold trailer, at a low pressure, to the positive displacement (PD) pumps. These pumps have variable speeds that allows them to produce different flow rates. Each pump is powered by an individual diesel engine via a transmission gearbox that is connected to the input shaft of the PD pump. All of these components (i.e. engine, transmission and pump) are jointly mounted on a trailer and transported as single unit. Individual triplex PD pump consumes up to 1,677 kW as shown in Fig. 7.

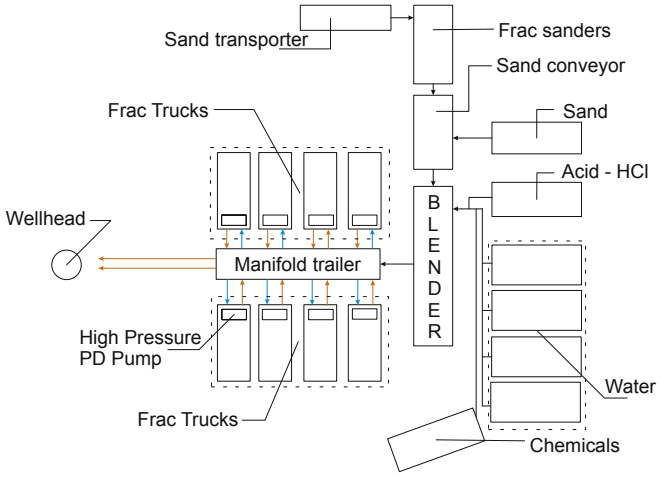


**Fig. 6.** Schematic diagram of the equipment on a hydraulic fracturing site. The flow path of the frac-fluid is from right to left of the schematic. In this schematic the red and blue lines represent high and low pressure lines, respectively. (For interpretation of the references to colour in this figure legend, the reader is referred to the web version of this article.)

Fig. 6 illustrates a fracturing site layout. On the right side of the schematic all of the consumables are stored prior to being merged and mixed in a blender unit. As discussed earlier, fluid is then transferred via a manifold trailer that ultimately supplies each individual pump with frac-fluid.

## 6. Positive displacement pump

High pressure pumping equipment is required to pump range of volumes of frac-fluid (as shown in Table 1) to pressurize the well formation until the surrounding rock fractures. After fracturing has occurred, pumps are needed to propel and deposit proppant into the newly opened fissures in the rock to keep the formation open. Some pump types, such as centrifugal or rotary pumps, decline significantly in performance once operated outside the point of peak efficiency. However, PD pumps have a broader operating range and are able to provide both high flow rates and pressure for sustained periods. Generally, hydraulic fracturing operation use three or five cylinder pumps, (referred to as triplex and quintuplex respectively) [31]. A typical 3-cylinder pump is shown in Fig. 7.

The fundamental physics of fluid movement means that all pumps are designed to operate in predefined ranges as shown in

**Fig. 5.** Photograph of the site showing high and low pressure pipework connecting positive displacement pumps (right) to a manifold trailer (left) on hydraulic fracturing site. Photograph was obtained from south Texas.

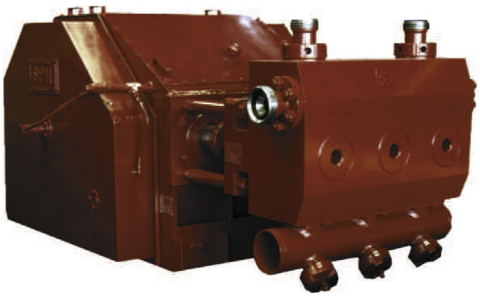

**Performance specifications:**

| Specification | Design | Value |
|---|---|---|
| Mech. horsepower | $HP_{\mathrm{rl}}$(kW) | 1,677 |
| Max. rod load capacity | $F_{\mathrm{max}}$(kg) | 108,214 |
| Max. engine RPM | $RPM_{\mathrm{eng}}$ | 1,950 |
| Gear ratio | $r_{\mathrm{g}}$ | 6.353:1 |
| Stroke length | $L$(m) | 0.204 |
| Plunger diameter | $D$(m) | 0.111 |
| Number of cylinders | $N_{\mathrm{cyl}}$ | 3 |
| Mech. efficiency | $ME$(%) | 90 |

**Fig. 7.** Left image shows typical 3-cylinder positive displacement pump employed in hydraulic fracturing [53]. To the right, the table details the performance specification of a typical pump.

Fig. 8(b). Operating PD pumps outside their design range can lead to premature failure caused by over stressing their structures [32].

In a hydraulic fracturing operation, pumps must be capable of providing both high pressure and (at different times) high flow output. The initial phase of a fracturing stage, known as the 'breakdown' phase, requires a high pressure to initially crack the rock (in Fig. 1 this is shown as phase 1 in the tenth minute of the stage). Although this duty lasts for only couple of minutes it is crucial to the success of the entire operation. The next part of the operation (phase 2 in Fig. 1) is referred to as the "fracture propagation" or "extension phase" [24]. In this phase, the cracks initiated in the 'breakdown phase' are propagated to create the desired fracture network necessary for maximum gas flow. Thus, this part of the hydraulic fracturing operation is also crucial as it directly determines the effectiveness of the well stimulation [25]. During this phase, the fluid pressure must be maintained at a lower level for a couple of hours while the flow rate increases between 4 and 6 times than in the breakdown phase. These flow rates are achieved either by increasing the speed of the pump, Fig. 8(b), or (when the performance limits of individual pumps are reached) by introducing additional pumps to the operation. An experimental study by Fan and Zhang (2014) highlights pressure variation due to different injection flow rate dynamics [33]. The negative effect of pressure oscillations are manifested in the form of unpredictable shale fracture development and are also damaging to the pumps and other process equipment generally used during hydraulic fracturing. Consequently the relationship between injection pressure and injection flow rate is critical for successful well stimulation.

As previously noted, there is no advantage to designing larger pumps (rather than requiring a greater number of pumps), since, in order to be portable, their size is limited by truck specifications in North America.

The functional constrains to the pump's design can be divided

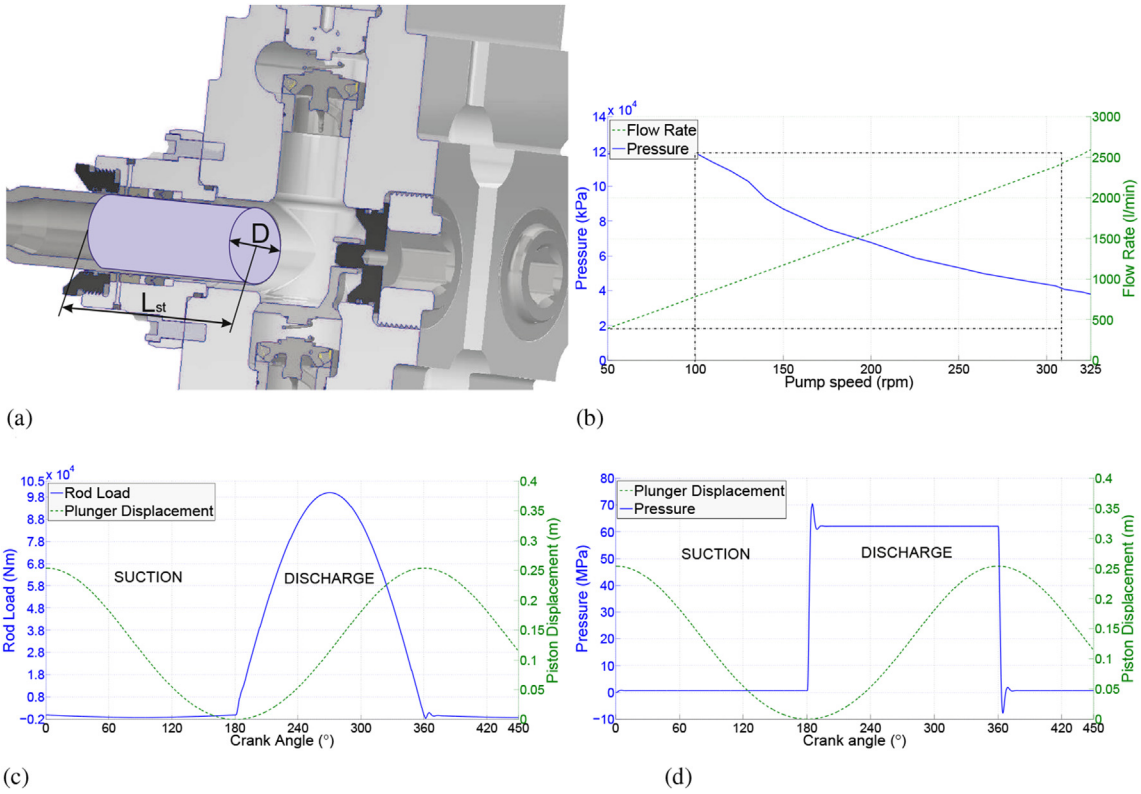


**Fig. 8.** Cross section of the positive displacement pump (a) with speed and pressure ranges (b). Typical cyclic variations in rod load (c) and pressure (d) seen during a single pumping stroke are shown.

into two categories, (i) fluid and (ii) strength limitations. In the following section we examine each in turn before considering how the system can be modelled.

### 6.1. Fluid limitations

Although fluid properties such as inertia or viscosity create theoretical boundaries for the flows and pressures that a pump can deliver, some of the most serious practical constraints are secondary to the movement of the fluid. For example, erosion is common even though pumps are manufactured from hardened-alloy steel (or in some cases stainless steel). This is because, as described in Section 5, the frac-fluid is a slurry of water, chemicals and proppants, that erode and corrode the pump components in two principal ways [34]:

- During the high flow operating regime sand and proppant particles cause erosion and wear in the fluid chamber.
- The addition of acid to the frac-fluid in some hydraulic fracturing operation causes corrosion that ultimately reduces the fatigue life of the pump.

Together, these processes wear the internal surfaces of the fluid chamber after a number of hours, leading to so called pump “wash out”. The effects of wear include leaking valves and deteriorated plunger seal. This limits the pressure at the outlet of the manifold trailer (i.e. the inlet of the pump's suction chamber). When the pressure drops below a critical threshold, cavitation problems occur in the fluid chamber (if suction pressure falls, cavitation can occur during the suction stroke) [35]. Perhaps the most serious consequence is that wear varies in proportion to the second or even third order of fluid speed [36]. In other words a small increase in fluid speed might have a dramatic increase in the rates of erosion and these issues lead to ineffective pumps, loss of volumetric efficiency and unbalanced operation. These design challenges must be overcome to achieve consistent flow pattern and avoid oscillation and vibration issues.

### 6.2. Strength limitations

The structural strength constraints of the pump can also affect operations in several ways. For example:

- Each pump has a pressure restriction due to the maximum rod load that its drive can transmit without buckling [34]. Each cylinder is controlled by a crankshaft that is powered from the diesel engine's driveshaft via a gearbox. However, due to the relative incompressibility of water, the pressure in the fluid chamber loads the piston early in the compression stroke, which in turn transmits loads to the entire cylinder assembly including the crankshaft [31].
- The pump housing is directly affected by periodic loads, particularly throughout the discharge stroke as shown in Fig. 8(c) and (d). The resulting strain frequently causes the pump housing to experience twisting and deflection.
- The cyclic loads on the structure, due to the drive mechanism, means that the power delivery (i.e. torque and speed) is non-linear [37]. The unsteady power delivery from the engine and transmission will impact on a pump's life through fatigue limits and shorter component life (e.g. bearings).

### 6.3. System modelling

A hydraulic fracturing pump is clearly a complex machine with many interacting elements. Consequently any efforts to optimize the process must take a system view and understand how changes in one area will affect others. The following section describes the analytical methods used to model the system.

Pressure in the cylinder is determined not only by the plunger area and displaced volume (i.e. plunger diameter and stroke), but also by the pressure resistance downstream (i.e. seen at the outlet). The downstream pressure is calculated based on different well characteristics (e.g. rock type and depth) rather than pump performance directly, and so it is necessary to use a fixed value for this variable.

The rod load (RL) calculations take into account the force applied to the plunger and the radius of the crankshaft as expressed by Eq. (11). Interacting parameters are shown in Fig. 9(a). The rod load limit defines the maximum achievable chamber pressure (P) and is dependent on the plunger area (i.e. plunger diameter (D)) on which the pressure acts and the crankshaft radius (R). The variation in rod load is shown in Fig. 8(c), and the load paths of the transmitted force illustrated in Fig. 9(a).

$$\begin{aligned} RL &= F \cdot R \cdot \sin\alpha \\ &= P \cdot \frac{D^2\pi}{4} \cdot R \cdot \sin\alpha \end{aligned} \tag{11}$$

Flow rate is a function of plunger stroke, speed and plunger diameter. All the values that alter the internal geometry of the chamber, such as stroke and plunger diameter naturally affect the swept volume and therefore the overall flow capacity. Flow rate is calculated using Eq. (12):

$$Q = \rho \cdot v \cdot \frac{D^2\pi}{4} \tag{12}$$

The frequency of the piston movement is affected by the rotational speed of the driveshaft. So in order to derive a flow equation

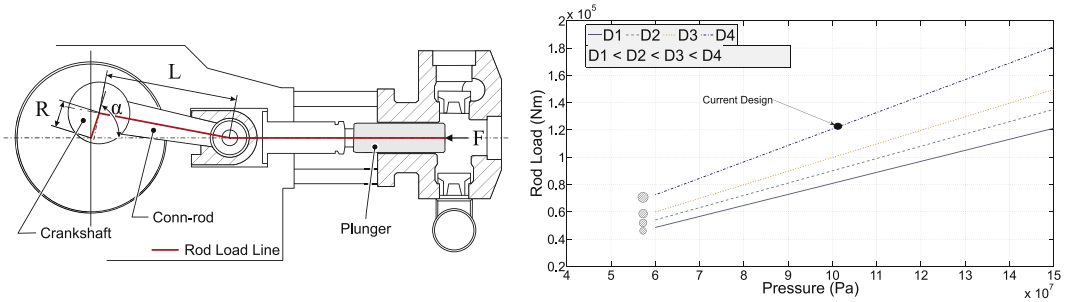


**Fig. 9.** The limiting factor in positive displacement pump design is the force (F) on the con-rod during compression stroke. Consequently, operating pressure can be increased by decreasing the plunger diameter (D).

it is necessary to introduce motion equations that describe the reciprocating movement of the piston.

$$f = \frac{60}{s} \tag{13}$$

For this purpose the classical crankshaft mechanism equations are used, including the following equation for the position of the piston with respect to the crank angle $\alpha$:

$$X(\alpha) = R \cdot \cos\frac{\alpha\pi}{180} + \sqrt{L^2 - R^2 \cdot \sin^2\frac{\alpha\pi}{180}} \tag{14}$$

where $R = L_{st}/2$ is the radius of the crankshaft equal to half stroke, $L$ is the length of the connecting rod, and the angle $\alpha$ is in degrees. Eq. (14) is modified to describe the displacement of the plunger starting from the bottom dead centre (BDC) to the top dead centre (TDC) with respect to time $t$:

$$X(t) = R \cdot \cos\alpha(t) + \sqrt{L^2 - R^2 \cdot \sin^2\alpha(t)} - (L - R) \tag{15}$$

where the angle $\alpha$ is related to time $t$ by the following equation:

$$\alpha(t) = \frac{\pi(t\omega - 180)}{180} \tag{16}$$

Further expanding Eq. (12) results in an expression for the total flow rate (Eq. (17)) where the density of the fluid, $\rho$, is assumed constant (at ambient pressure and temperature).

$$Q = \rho \cdot \frac{dX(t)}{dt} \cdot \frac{D^2\pi}{4} \tag{17}$$

The pump's power consumption is a product of speed, force and the number of cylinders. Additional factors such as plunger friction force ($F_f$) and plunger inertia ($F_{in}$) are included in the total power Eq. (18):

$$\begin{aligned} P_{tot} &= n \cdot v \cdot \left(F_{in} + F + F_f\right) \\ P_{tot} &= n \cdot v \cdot \left(m \cdot a + p \cdot A + F_f\right) \end{aligned} \tag{18}$$

These equations describe the interaction of the design parameters of a positive displacement pump and lay foundation for exploring alternative configurations. In the subsequent sections the paper will examine alternative concepts based on the current design and quantify the potential impact of changes to the performance.

## 7. Pump design space analysis

An optimised design needs to incorporate both high pressure capability and sufficient flow capacity. An increase in volume capacity will lead to better time management on site.

It is clear that pumping pressure, speed, plunger diameter, stroke length and rod load all interact, so what is the best combination of values? And could there be scope within the design space to select values that result in a smaller more compact pump which are appropriate for European transport specification, environmental and societal constraints? To investigate this hypothesis a numerical model was used to systematically explore the system's design space with the aim of optimizing the size of the reciprocating components for a given pressure and flow.

This process of multivariable analysis has five steps:

1. Identify current design specification
2. Create a computational model of the system
3. Coarse grid exploration of design space
4. Identification of sets of candidate parameter values for system improvement
5. Finer grid search through Monte Carlo optimisation

The following sections detail each step of this process.

### 7.1. Current design

Identifying parameters values associated with current equipment is the first step in development of the full multivariable analysis. Fig. 10 shows a hydraulic horsepower power curve and the key design parameters used as a starting point for the analysis presented. The red dot represents the single operating state that will be used as a representative example of pump capabilities.

### 7.2. Model

A mathematical model was developed to explore the design space using the parameters in Table 2.

The system's outputs are rod load (i.e. cylinder pressure) and flow rate. The rod load is a cyclic function dependent on the plunger placement during the operating phase. The rod load

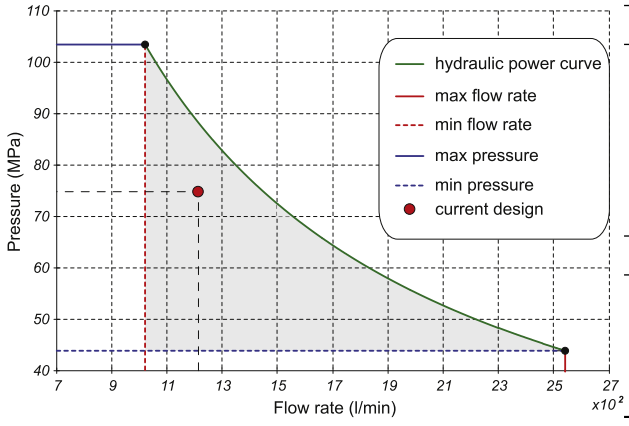


| Current Design | | |
|---|---|---|
| Nom | Input | |
| D | Plunger Diameter (m) | 0.111 |
| R | Crank Radius (m) | 0.102 |
| L | Conn-Rod Length (m) | 0.65 |
| X | Speed (rpm) | 200 |
| m | Plunger mass (kg) | 400 |
| $m_{tot}$ | Total mass (kg) | 1200 |
| C | Number of Plungers | 3 |
| Nom | Output | |
| F | Force (N) | $7.2 \cdot 10^5$ |
| $F_f$ | Friction force (N) | 300 |
| p | Pressure (MPa) | 75 |
| Q | Flow Rate (l/min) | 1248 |
| $P_{tot}$ | Power(MW) | 1.350 |

**Fig. 10.** A pump's operating range is the area below its characteristic hydraulic power curve. Identifying a single operating point (i.e. current design) allows pump operation to be discretized and a multivariable analysis to be carried out. The table on the right details the specification of the current design.

**Table 2**
The ranges of values used in the initial coarse grid exploration analysis to identify the range of performance values in current pump design.

| Input | | | | | Output | |
|---|---|---|---|---|---|---|
| Parameter | Var. | Current design. | Min | Max | Parameter | Var. |
| Plunger | | | | | | |
| Diameter (m) | $D_i$ | 0.111 | 0.008 | 0.134 | Rod Load | $RL$ |
| Crank | | | | | | |
| Radius (m) | $R_j$ | 0.102 | 0.01 | 0.164 | Flow Rate | $Q$ |
| Con-rod | | | | | | |
| Length (m) | $L_k$ | 0.650 | 0.05 | 0.750 | | |
| Speed (RPM) | $X_l$ | 300.0 | 100.0 | 700.0 | | |
| Number of cylinders | $C_o$ | 3 | 1 | 12 | | |

variation over one pumping cycle is shown in Fig. 8(c) and modelled by Eq. (19).

$$RL\left(IN_{ijklo}\right) = \frac{D_i^2\pi}{4}\cdot R_j \cdot \sin\left(\frac{2\pi\cdot X_l\cdot t}{60}\right)\cdot p \tag{19}$$

The flow rate varies with the cyclic piston movement during the compression stroke. Integrating the discharge flow gives a single value that is associated with the internal displaced volume (Q), Fig. 8(a). Thus the total displaced volume from three cylinders over specified time (t) is defined by Eq. (20) (assuming no losses in the volumetric efficiency).

$$\begin{aligned} Q\left(IN_{ijklo}\right) = 3\cdot\frac{D_i^2\pi}{4}\cdot R_j\cdot\cos\left(\frac{2\pi\cdot X_l\cdot t}{60}\right) \\ +\sqrt{L_k^2 - R_j^2\cdot\sin\left(\frac{2\pi\cdot X_l\cdot t}{60}\right)^2}\cdot 998.2 \end{aligned} \tag{20}$$

### 7.3. Coarse grid exploration study

Every combination of the five input parameters was generated (Eq. (21)) [38] by incrementally varying them between minimum and maximum values that represent physical or functional limits to that quantity. Table 2 shows the values used in the coarse grid analysis. The step size is 1% of the range.

$$IN_{ijklo} = \left(D_i R_j L_k X_l C_o\right)\Big|_{i=1}^{i=n_1}\Big|_{j=1}^{j=n_2}\Big|_{k=1}^{k=n_3}\Big|_{l=1}^{l=n_4}\Big|_{o=1}^{l=n_5} \tag{21}$$

The values of connecting-rod length and crank radius are constrained by the kinematic limitation. Therefore, some values of $IN_{ijklo}$ were excluded and Eq. (22) defines the combinations of parameters excluded by this design constraint.

$$\begin{aligned} IN_{ijklo} = \left\{ D_i, R_j, L_k, X_l, C_o \middle| \frac{L_k}{R_j} \le 5.2 \text{ and } \frac{L_k}{R_j} \ge 2.8 \right\} \\ \text{Where :} \\ i = 1\ldots n_1, j = 1\ldots n_2, k = 1\ldots n_3, \\ l = 1\ldots n_4, o = 1\ldots n_5. \end{aligned} \tag{22}$$

The final multivariable space of possible PD pump designs can be represented as an array of input and output values, Eq. (23).

$$\begin{pmatrix} IN_{11111} & RL(IN_{11111}) & Q(IN_{11111}) \\ \vdots & & \\ IN_{1111n_1} & RL(IN_{1111n_1}) & Q(IN_{1111n_1}) \\ \vdots & & \\ IN_{n_1n_2n_3n_41} & RL(IN_{n_1n_2n_3n_41}) & Q(IN_{n_1n_2n_3n_41}) \\ \vdots & & \\ IN_{n_1n_2n_3n_4n_5} & RL(IN_{n_1n_2n_3n_4n_5}) & Q(IN_{n_1n_2n_3n_4n_5}) \end{pmatrix} \tag{23}$$

We adopted a discrete fixed step approach because incremental changes to the output (i.e. no step changes) makes the impact of the parameters easier to distinguish.

### 7.4. PD pump design space results

The results show that, as expected (Fig. 9(b)), a wider plunger is associated with a relative increase in Rod Load as the pressure rises. Similarly, it is unsurprising that the stress on the crankshaft increases as the plunger area increases, and this stress ultimately limits the maximum operating pressure. Since changes in the design parameters (i.e. plunger diameter, crank radius and con-rod) will result in different output characteristics, four areas of output characteristic can be identified in Fig. 11.

- Large plunger area and low speed (top left corner of Fig. 11): low flow and high rod load performance.
- Medium - large plunger area and a range of speeds (top right corner of Fig. 11): large variations in rod load and flow rate.
- Small - medium plunger area and mid to low speed (bottom left of Fig. 11): relatively low rod load and low flow rates.
- Small - medium plunger area and high speeds (bottom right of Fig. 11): relatively low rod load and high flow rates

For each area, the parameters can be expanded to explore in more detail the possibilities of different pump designs.

### 7.5. Monte Carlo optimisation

The aim is to maximize flow rate while minimising rod load; an optimised design needs to be able to deliver both high pressure capability and sufficient flow capacity, since the flow rate of the pump is a significant factor in the overall time taken to complete a stage.

The next step is to identify whether the same level of performance can be obtained with the improvements in the equipment footprint. This is achieved by running another simulation with the system's objective functions defined. This second phase of the multivariable analysis involves a more detailed exploration of the reduced parameter space identifier through the previous coarse grid search, (Section 7.3).

Optimisation was done using a Monte Carlo analysis with filtering to provide information about the model sensitivity and parameter ranges around optimum values. The process has three distinct steps:

1. Explore the reduced parameter space using a Latin Hypercube [39],
2. Filter and weighting the simulation according to the chosen criteria,
3. Infer the posterior distributions for each parameter according to the calculated weights.

The filtering has been conceived in order to explore the possibilities for improving current design while maintaining the same output performance (i.e. flow rate). The flow rate represents the

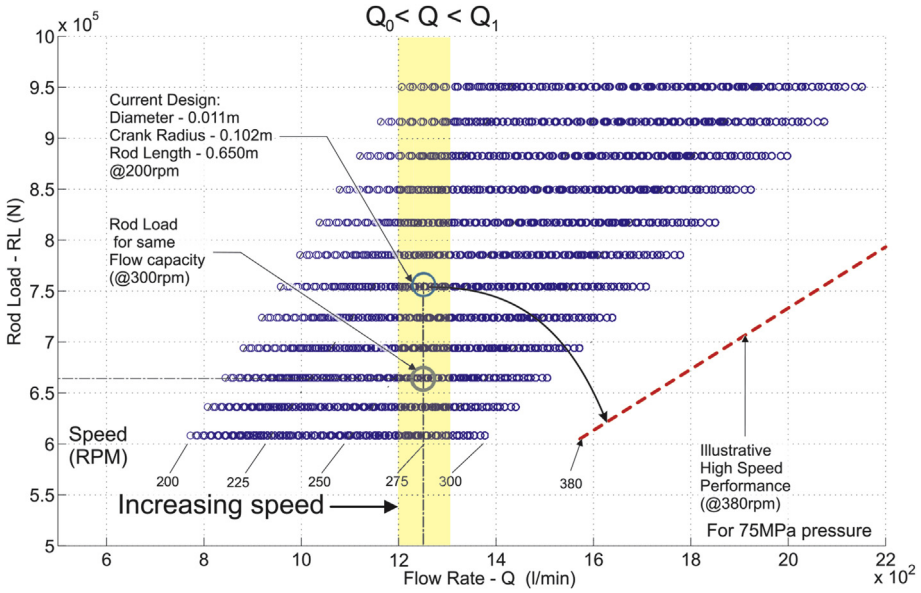


**Fig. 11.** In this figure the current operating range was located with pump parameter plot for constant pressure. Each horizontal line consisting of blue points is associated with a different plunger diameter. Similarly, each sloping vertical line presents a different speed parameter. The dashed red line indicates how speed increase would minimise rod load for the same flow rate. The shaded yellow area presents the boundary limits for the next phase of the optimisation. (For interpretation of the references to colour in this figure legend, the reader is referred to the web version of this article.)

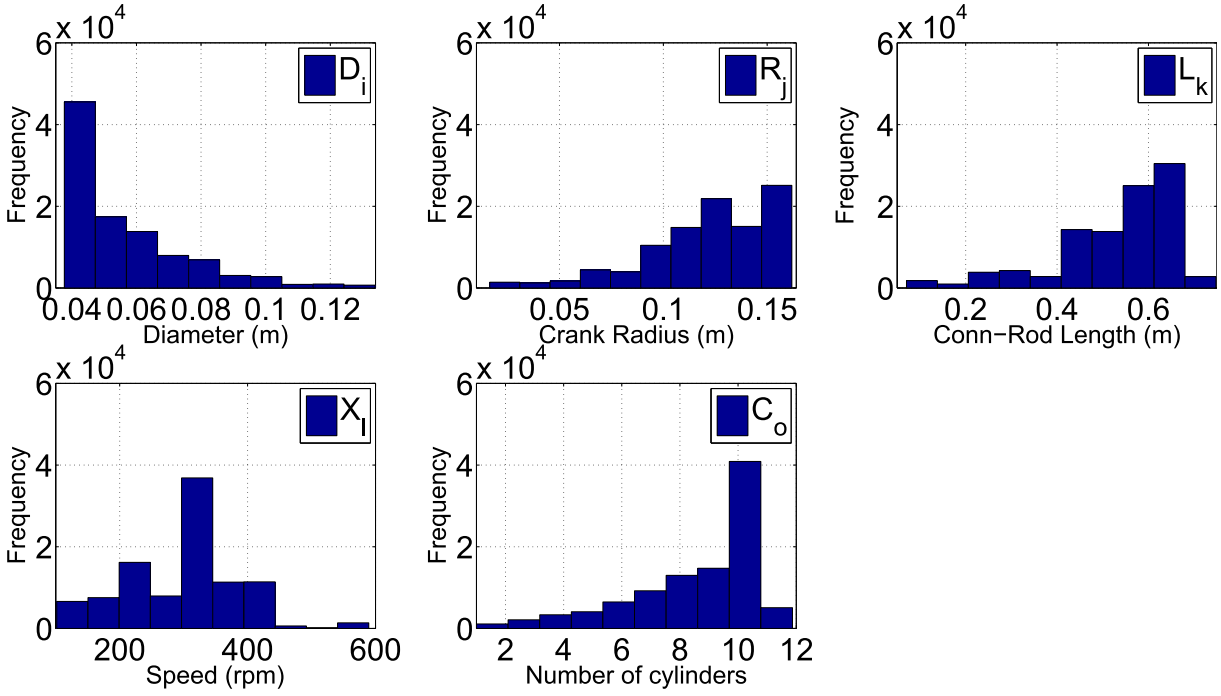


**Fig. 12.** Histograms of the evaluated data for the five key pump design parameters ($D_i$, $R_j$, $L_k$, $X_l$, $C_o$) identify optimum values for best performance. The optimised model adopts the peak value in each of the five histograms.

first objective function, boundaries for (Q(i)) must be defined and only simulations returning flow rate values within the limits defined in Eq. (24) are retained.

$$Q_0 < Q\left(IN_{ijklo}\right) < Q_1 \tag{24}$$

Values $Q_0$ and $Q_1$ present acceptable range for the new design. These values are centred around the current operating range shown in Fig. 10, where $Q = 1{,}472$ l/min.

The input vector weighting defines a score (or weight) to each retained simulation according to the probability that it would return the minimum rod load (i.e. the optimum). The rod load Eq. (25) is the second objective function designed to weight combination of parameters according to minimum value.

$$f\left(RL\left(IN_{ijklo}\right)\right) = \left(\frac{1}{RL\left(IN_{ijklo}\right)}\right)^{N} \quad (25)$$

The posterior distributions were inferred by sampling with replacement the simulation input vectors, defined by the initial Latin Hypercube design, using probabilities proportional to the calculated weights. The optimal value and range for each parameter were calculated by taking respectively the mode and the 95% confidence interval for such distribution. The value of coefficient N (in Eq. (25)) was elected following a number of model trials. $N = 2$ was deemed to adequately define the posterior distribution.

The optimised values of the PD pump parameters are presented in Table 3. In addition to the qualitative benefits the mechanical structure of the pump that will result from the reduction in plunger diameter the analysis suggests a 4.6% energy saving. Detailed sensitivity analysis for studied parameters is presented in Fig. 12.

### 7.6. PD pump design space discussion

Fig. 11 illustrates a projection of the six dimensional design space. Each point of the plot represents one set of input parameters. Two of the current functional (Flow Rate - Q) and physical (Rod Load - RL) limits are shown on the graph to illustrate the boundaries of the current design.

Lines for constant pump speeds (RPM) are marked in black, in increments of 25 rpm for the appropriate speed limits. The red dashed line in 11 illustrates the impact of increasing the maximum pump speed by roughly 33% to 380 rpm.

Since pressure is directly dependent on the rod load limit, decreasing rod load requirements could achieve an increase in performance. Similarly, the same pressure output could be attained by optimizing the crankshaft to save extra weight and size.

The multi-variable model presented gives the initial basis for the optimised pump design. The advantage of this approach is the overall flexibility of the model and the ability to quickly assess design configuration independent of physical limitations.

## 8. Hydraulic fracturing: case study

The design space presented in Section 7 has been explored for solutions that minimise power requirements while delivering appropriate performance. To investigate the impact of the proposed design on a hydraulic fracturing process case studies are used. The mechanical properties associated with a rock formation in Woodford Basin (Oklahoma) are summarized in Table 4[40]. Zhang et al. (2014) [41] presents an “energy” study for which typical hydraulic fracturing was modelled using the STIMPLAN software [42]. The reservoir properties in their study are similar to the recorded reservoir data used in our model. The analysis in this paper will use a single stage in “Well 3's” stimulation program, shown in Table 1, as a representative example for energy estimation.

### 8.1. Pumping period

The pumping rate for a single stage of hydraulic fracturing will be determined in advance of the propagation phase. The overall time is influenced by the size (width, depth, length) of the well and the mechanical properties of the rock (determined by rock type, depth). For this case study the time of the stage is set to 210 min. Experience in North American shale reservoirs suggest that this estimate is towards the upper limits of a pump stage, i.e. longer than the average time required.

### 8.2. Pump pressure

The formation breakdown pressure ($p_b$) for our theoretical well can be derived from Eq. (6) using the parameters in Table 4, and is approximately 62 MPa.

$$p_b = 3\left[\left(\frac{\upsilon}{1-\upsilon}\right)(\sigma_V - \beta p_r) + \beta p_r\right]H - \sigma_{Hmax} + T - \beta p_r H = 62 \text{ MPa } (9,000 \text{ PSI}) \quad (26)$$

For our case study, propagation pressure ($p_p$) is therefore approx. 43 MPa (assuming a 30% reduction of the breakdown

**Table 3**
Optimised PD pump parameters identified by the multivariable analysis indicates a 4.6% energy saving.

| Comparison between two design states | | | | | | | | | |
|---|---|---|---|---|---|---|---|---|---|
| Nom | Input | Current | Optimised | % Change | Nom | Output | Current | Optimised | % Change |
| D | Plunger Diameter (m) | 0.111 | 0.037 | −194% | F | Force (N) | $7.2\cdot10^5$ | $8.3\cdot10^4$ | −860% |
| R | Crank Radius (m) | 0.102 | 0.155 | +52.6% | $F_f$ | Friction force (N) | 300 | 50 | −600% |
| L | Con-rod Length (m) | 0.650 | 0.640 | −1% | p | Pressure (MPa) | 75 | 75 | – |
| X | Speed (rpm) | 200 | 334 | +67% | Q | Flow rate (l/min) | 1248 | 1207 | −3.2% |
| n | Number of plungers | 3 | 11 | +260% | $P_{tot}$ | Power (MW) | 1.350 | 1.288 | −4.6% |

**Table 4**
The case study shale formation properties are listed. This case study is used to quantify the potential impact of the optimal pump design. Values for North American shale are used due to lack of available data for European shale.

| Formation details | | Well 3 - shale properties | | |
|---|---|---|---|---|
| Formation | Woodford | Parameter | Variable | Value |
| Lithology | Shale | Depth (m) | H | 4649 |
| Top MD(m) | 3522 | Poisson's Ratio | $\upsilon$ | 0.2 |
| Bottom MD(m) | 4649 | Vertical stress (kPa/m) | $\sigma_v$ | 0.2 |
| Pore pressure (kPa) | 39,330 | Poroelastic constant | $\alpha$ | 0.8 |
| Pore pressure (ppg) | 9.8 | Pore pressure (kPa/m) | $p_r$ | 11.51 |
| Fluid content | gas | Max. Horizontal stress (kPa) | $\sigma_{Hmax}$ | 72,180 |
| Frac gradient | 0.72 | Tensile strength (kPa) | T | 1722 |
| Total pump power requirements (kW) | 14,155 | | | |
| Breakdown pressure (kPa) | 62,100 | | | |

pressure). This pressure will be maintained throughout the propagation stage.

### 8.3. Flow rate

The total volume of liquid required for the fracturing operation (over the chosen 210 min period) needs to be estimated to determine the magnitude of the flow rate. The total volume is the sum of the volume of liquid needed to fill the bore, calculated using Eq. (10) and the volume needed to push the proppant into the rock fissures. In order to calculate the volume of the production well casing it is necessary to define both the measured depth of the well and casing diameter. A standard production casing diameter is $2^{7}/_{8}$" (imperial units are industry standard). Using Eq. (10) calculated volume of the well bore is 19,500 l. The combination of the calculated casing volume and the recorded field data suggests the total volume of pumped fluid for this example well stage is approximately 2.45 Ml. It is interesting to note that casing volume is only 0.7% of the overall fluid needs. In other words the casing volume is negligible compared to the quantity of fluid pumped into the rock during the fracture propagation stage.

The entire hydraulic fracturing process can be modelled using the calculated volume requirement parameter and formation breakdown pressure.

### 8.4. Pump requirements

The pump pressure needed to fracture this well (62 MPa) is obtained from the mid-range of the performance curve of the pump, Fig. 8(b), confirming that the optimised pumps will be capable of delivering this required pressure to the wellbore. Given that the volume of liquid needed is approximately 2.45 Ml and the time to deliver this volume is 210 min, the pumping rate must be 16,000 l/min. To generate this flow, a total of 14 positive displacement pumps would have to be used in parallel requiring power of 25 MW.

### 8.5. Environmental footprint

Since we have determined the overall fluid volume needed to fracture a single stage in the example well, and the number of pumps required to achieve these flow rates, it is important to consider the physical issues of delivering the equipment to site. One of the principal impacts on the local community is nuisance (noise, traffic) and air pollution from trucking [18]. Additionally, road traffic accidents (and subsequent spillages of e.g. frac-chemicals) are one of the most likely risks to the environmental posed by hydraulic fracturing operations [7]. Thus infrastructure delivery to site has important implications for the environmental and social impact of hydraulic fracturing activities, which operators should seek to minimise.

Further, the pumps require a great deal of power to operate. This power is usually provided by diesel generators (with associated air pollution issues). Minimising the number of pumps would not only reduce transport strains but also the overall power requirements of the pad. All the units (e.g. water tankers, sand tankers, mixing and hydration units, pumps, pipework and control centre) on the hydraulic fracturing site are mounted on trailers that are limited in size by transport legislation. A tanker, in accordance with EU road legislation [43], is able to transport a maximum of 32,000 l of water or petrol (this volume is limited by mass restrictions). For this case study, 78 water tankers would be needed to transport the required amount of fluid (outlined in Section 8.3) to the well location. There will be additional trucks to transport the frac-chemicals and proppant - the volumes of which will be proportional to the total fluid volume pumped. However, the volume of both sand and chemicals required are an order, or even two orders of magnitude smaller than the water needed.

Due to strict road (load) and transport regulations, pump manufactures and final assembly companies are very conscious of the physical size of the frac-trucks. The EU Council Directive 96/53/EC [43] specifies a maximum authorized dimension for national and international road traffic. Similarly pump assembly manufactures specify maximum overall dimensions of their units [44] to fit the size limits. These limits (designed for the North America) are approaching the very limit of the acceptable range for the European roads.

### 8.6. Case study summary

The mechanical properties of the rock and the time scheduled for each stage of the hydraulic fracturing largely dictates the amount of pumping hardware required. While it may be preferable to process a stage in a shorter time (for economic reasons and to reduce the period disturbance to local environment), doing so would require more pumps in operation at a given time. For the purpose of this study, an example hydraulic fracturing process from North America has been adopted. For this operation, 2.45 Ml volume of liquid must be delivered to the rock over a period of 210 min, requiring pump flow rates of 16,000 l/min. All the positive displacement pumps on the site individually must be capable of exceeding the formation breakdown pressure (62 MPa in this case study).

After the breakdown phase, pumping shifts from a low speed, high pressure regime to a high speed, high flow rate (the propagation phase). The pumping profile associated with this case study is shown in Fig. 13, which details the fluid pressure, flow rate and fluid density requirements. The case study demonstrates that an optimised pump could deliver adequate pressures and flows for a typical job.

The number of pumps and their duty cycle can be used to determine the power needed to run the site. These will determine both the traffic and environmental footprint of a single hydraulic fracturing stage. All the other variables present in the process such as sand and chemicals are affected by the size of the reservoir and the total water requirements.

## 9. Discussion

In order to develop shale gas resources in Europe it is necessary to establish energy efficient operations with minimal environmental and social impact. Europe has committed to carbon emissions reductions targets, and so should the shale gas industry be developed, it is important that it is done so in a way that minimised life-cycle emissions of the process. The slower planning and permitting process in the EU (compared to the North American) and differences in the geological resource [16], make it particularly important to make the process as economically efficient as possible so as to ensure profitability.

If one assumes that basic mechanism of the stimulation process remains the same then any improvements must come from the changes to the equipment. The preceding sections have shown how a reduction in cylinder diameter could result in an energy saving, however, it would also allow mass savings. The smaller diameter will result in lower hoop stress around the cylinders and so allow reduction in the mass. Consider, for example, the economic benefits associated with reduction in size of the equipment:

- Truck Size: Pressure pumping equipment and water are transported to site by heavy duty trucks. The North American frac-truck is near the limits of acceptance for EU roads. Therefore,

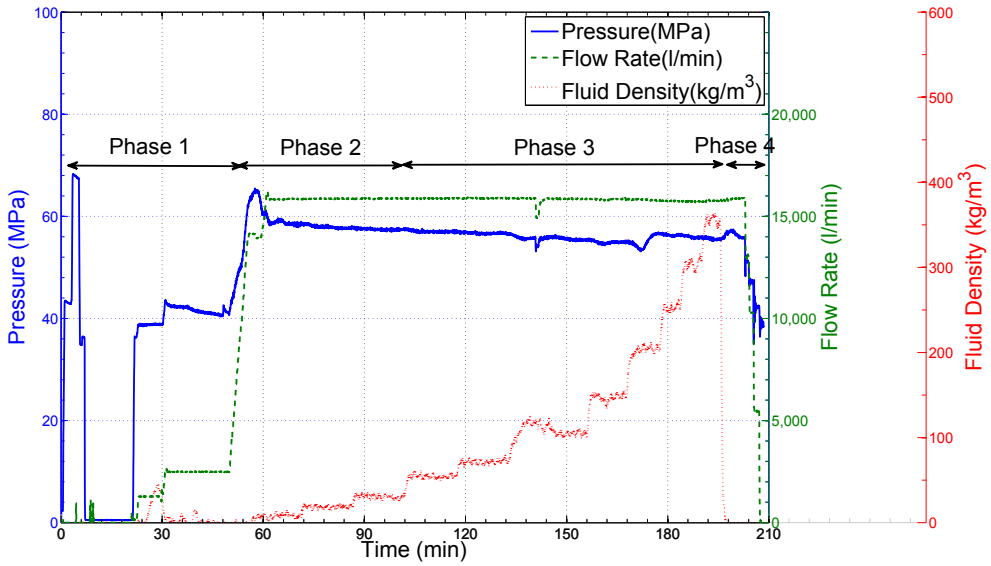


**Fig. 13.** Experimental case study values (obtained from North American well stimulation operations) used to determine pumping requirements for hydraulic fracturing [40].

more compact equipment will result in better utilization of transported weight and volume. The material costs during pump and truck manufacture could also decrease due to reduced mass.
- Energy Consumption: Pumping is powered by industrial diesel engines. These units have significant fuel consumption and emission generation. Consequently, a reduction in the power requirements would in turn reduce fuel needs and the pollution/noise associated with 6–20 large industrial engines running simultaneously in a full load condition.
- Carbon Footprint: The embedded carbon in the pump and pump truck will be lower if they are reduced in material mass. For example, 1.9 tonnes of CO2 are emitted for every tonne of steel manufactured in 2014 [45]. This is discussed in Section 9.2

The preceding discussion has established that the pumps used for hydraulic fracturing are required to operate in several modes, each with different performance requirements:

- Pad Mode (Moderate Pressure - High Flow): to fill the well bore with fluid prior to pressurization.
- Breakdown Mode (Very High Pressure - Moderate Flow): to create the fracture pressure at which cracks are initiated.
- Propagation Mode (Moderate Pressure - High Flow): to extend the length and width of the cracks.

The general approach established in North America is to use the same pump (running at different speeds) for all three modes. Consequently, all the pumps on a hydraulic fracturing site are designed to have operating profiles that, dependent on the drive speed, can provide both high pressures and high flows (although never at the same time). A consequence of this “mono-pump” approach is that *all* the power-ends and *all* the fluid-ends are physically larger than they need to be. For example:

- When operating in Pad Mode: Large diameter plungers would be preferable to generate high flows with a large swept volume running at a moderate speed. The pressure during the pad creation is low so components can be sized to carry modest mechanical loads.
- When operating in Breakdown Mode: Small diameter plungers would be ideal because the flow rate requirements are low so only a relatively modest swept volume is needed. The physical size of the other components would also reduce because the mechanical strength requirements will scale with the load seen by the drive (aka power-end) which in turn will be the product of plunger area and pressure.
- When operating in Propagation Mode: Plunger diameter must be optimised to match the power curve of the drive with the pressure and flow characteristics of the pump.

### *9.1. Optimizing PD pump parameters to minimise mass and energy requirements*

The multi-variable analysis of the design space illustrated how pump design parameters interact. One direction of design improvement is suggested by the history of mechanical engineering. In the past dramatic improvements to size, energy and emission have resulted from increases in the speeds of reciprocating systems. The mechanical benefits of increased speed are well illustrated by the development of the internal combustion engine. For example, around early 1900s Rolls Royce car engines were significantly larger in size (4,118 cc, 4 cylinder) but produced only 20 bhp. In contrast, today's Formula 1 engines are 1,600 cc turbocharged V6 machines and produce up to 600 bhp [46]. Although new engines have incorporated improvements in electronic regulation, valve timing and precision manufacturing, one of the key change is the output speed of the engine. Compared to Rolls-Royce engines from 1900s which were outputting 1000 rpm today's Formula 1 engine are revving up to 15,000 rpm.

By applying a similar approach to PD pump the authors have assessed the potential for redesign of current technology to maximize efficiency. Consider how rod load and speed would have to vary to maintain a constant flow as the plunger diameter is reduced:

- Reducing plunger diameter by 10% implies the pump speed must increase by 23% to provide the same flow but the rod load will reduce by 19%

- Reducing plunger diameter by 23% implies the pump speed must increase by 56% to provide the same flow but the rod load will reduce by 36%
- Reducing plunger diameter by 30% implies the pump speed must increase by 100% to provide the same flow but rod load will reduce by 50%.

Such reductions in rod load and the associated hoop stress in the cylinder (associated with reduced diameter) would significantly reduce the stresses in the pump. However, increased fluid speed will also be associated with increased wear so the creation of high speed pumps for hydraulic fracturing would have to be associated with the adaption of technology that allowed sand and frac-fluid to be introduced after the pumps. Such a change would reduce erosion and corrosion rates that currently occur due to the abrasive fluid moving through the pump.

### 9.2. Environmental and social impacts

As discussed in Section 1, the direct and indirect greenhouse gas emissions associated with the construction and completion of the shale gas well can be significant [16]. To reduce the carbon intensity of these activities, and thus the environmental footprint of shale gas, operators could seek to, for example, reduce the surface area of the well pad, the size and mass of surface infrastructure, transport distances of materials, and the pad power requirements. It is also important that these activities minimise the disruption to local communities. Impacts to local air quality, noise and traffic issues are associated with hydraulic fracturing, and, where possible, these impacts should be mitigated or reduced. Noise and emissions ($CO_2$, SOx, NOx, CO and other pollutants) mostly source from the transport and operation of site equipment, as well as site materials. Our modelling specifically optimised for efficiency, since more efficient pumps will have environmental benefits and social benefits. For example, the enhanced pump design that we present here could reduce the environmental footprint of the high pressure fluid pumps on site during the well completion stage, and any future re-fracking if required during the operation of the well in several ways:

1. The enhanced pump design is more efficient than the current pump design. This will in turn reduce the fuel requirement for a hydraulic fracturing job, and thus the emissions from fuel combustion. Not only will this reduce the greenhouse gas emissions associated with the operation, but also pollutant emissions that affect local air quality and impacts on on-site workers and communities local to the developments.
2. The enhanced pump design may be more reliable because of the reduce load on the components. Increased pump reliability could demand less standby pumps (in case of wash-out, erosion), again reducing the bulk materials for transport and the associated issues (emissions and noise). Improved reliability may also decrease the risk of surface spillages and leaks from pump wash out.

In an attempt to quantify the reduction in direct greenhouse gas emissions and other pollutants from improved pump efficiency, we can apply the 4.6% reduction in energy requirements to the on-site diesel consumption during typical hydraulic fracturing. A study by Rodriguez et al. (2013) report fuel consumption and on site emissions for 14 pumps operating on a 17 stage well at two hydraulic fracturing sites in North America; in the Marcellus and the Eagle Ford shale. Diesel consumption for these operations was estimated to be 95100 $m^3$ respectively [19]. The study also calculated on-site emissions of $CO_2$, CO, SOx, NOx and other pollutants and, as previously noted, found that powering the pumps contributed 90% of total emissions on site.

Thus, introducing a pump power saving of 4.6% would, according to the values measured by Rodriguez et al. (2013), save up to 4.6 $m^3$ of diesel per frac. If the EIA figures [47] for diesel price in 2012 (the period that field data was collected) are applied, this would save operators $4,000 per frac. Reducing the quantity of diesel combusted to power the pumps would also decrease the quantities of nitrous oxides emitted by 8.16 kg, HC by 0.3 kg, carbon monoxide by 1.5 kg and particulate matter by 0.27 kg. On site diesel consumption will vary site by site, and frac-by-frac, and so in the absence of other published data information, these values are only indicative. Regardless, improved pump efficiency can offer significantly reduced emissions and operational cost, illustrating the multi-faceted value of optimised design.

We did not optimize the pump to reduce other parameters such as pump mass and dimensions. However, the reduced plunge diameter may in turn reduce the mass and dimensions of the pumps, which will bring associated environmental and economic benefits. Future research should explore the changes to these parameters further, but here we qualitatively discuss the potential environmental benefits from these changes, for example:

- Reducing the mass of the pump will in turn reduce the embedded carbon of the equipment (less steel required during pump manufacture), and the emissions associated with transporting the pump to the site. This would reduce the carbon footprint of pump transport and also reduce the impact of their transport on local air quality. Further, lighter pumps could reduce the damage to local roads that arises from transporting heavy goods and can cause disruption to local livelihood and noise problems.
- Reducing the size of the pump could enable smaller trucks to transport the pumps, further reducing the fuel requirements for pump transport and potentially also reducing the pad area required for the hydraulic fracturing pump array.

The environmental footprint of shale gas operations is also affected by the source of power for the site [1]. The utilization of recovered gas to power the frac site can bring economic and environmental benefits [48] improving air quality and reducing site noise and traffic (reduced need for fuel trucks). Leading industrial engine manufacturers have already made this technological development by promoting "hybrid" powered stations [49] and dual fuel systems [50] that can use both natural gas in addition to conventional diesel fuel. Should the improved pump design be powered by gas, the nuisance impacts for local communities would be reduced further.

## 10. Conclusion

Shale gas extraction by hydraulic fracturing is an emerging industry in Europe, whereas it is well established in North America. In North America, the engineering choices implicit in the current designs of high pressure fluid pumps did not focus on minimising the physical and environmental footprint of the operation, since their design was largely in response to the need for hydraulic fracturing at higher pressures and greater depths. However, there is no reason why the site machinery deployed in the EU has to be identical to that used in North America. In this paper, we consider how more efficient pumps could be designed that meet functional and environmental specifications.

We find that there is considerable scope for redesign of current hydraulic fracturing technology. The analysis presented in this paper has demonstrated that a 4.6% improvement in energy efficiency

is theoretically obtainable by optimizing the relative proportions of the established design. In 17 stage hydraulic fracturing process, as reported by Rodriguez [19], such a change would:

- Reduce diesel fuel consumption by 4,500 l (saving $4,000 per frac),
- Reduce *CO* emissions by 1.5 kg,
- Reduce NOx emission by 8.16 kg, and other associated pollutants occurring in diesel combustion;

Qualitative discussion of the potential environmental and social implications of these changes suggest that more efficient, and potentially more reliable pumps, have a lower associated environmental impact in terms of direct and indirect greenhouse gas emissions and also nuisance impacts for local communities, including air quality, noise and traffic. We also identify that further improvements could be made by reducing the pump mass and size. Quantification of these benefits is a subject for future work.

In conclusion, this paper has outlined engineering rationale for creating a compact, low energy hydraulic fracturing technology which is important for shale gas operations and other geological resources. Optimum pump design ought to be established for better process management and enhanced efficiency of the system. In short, key economic and environmental advances in hydraulic fracturing could come from innovate design and improved operation of site equipment.

## References


[1] King GE. Apache, Hydraulic fracturing 101: what every representative environmentalist regulator reporter investor university researcher neighbor and engineer should know about estimating frac risk and improving frac performance in unconventional gas and oil wells. In: SPE hydraulic fracturing technology conference. Society of Petroleum Engineers; 2012. http://fracfocus.org/sites/default/files/publications/hydraulic_fracturing_101.pdf.

[2] Younger PL. Hydrogeological challenges in a low carbon economy. Q J Eng Geol Hydrogeol 2014;47(1):7–27. http://eprints.gla.ac.uk/87691/.

[3] International Energy Agency - IEA, Golden rules for a golden age of gas, world energy outlook special report on unconventional gas, Paris, France, http://www.worldenergyoutlook.org/media/weowebsite/2012/goldenrules/weo2012_goldenrulesreport.pdf.

[4] Biresselioglu ME, Yelkenci T, Oz IO. Investigating the natural gas supply security: a new perspective. Energy 2015;80:168–76. http://dx.doi.org/10.1016/j.energy.2014.11.060.

[5] ASME, Fracking: A Look Back by Michael MacRae, [online], Accessed: 17.04.14, https://www.asme.org/engineering-topics/articles/fossil-power/fracking-a-look-back.

[6] EEC. A brief history of hydraulic fracturing [online]. 2012. Accessed: 17.04.14, http://www.eecworld.com/services/258-a-brief-history-of-hydraulic-fracturing.

[7] Mair R, Bickle M, Goodman D, Koppelman B, Roberts J, Selley R, et al. Shale gas extraction in the UK: a review of hydraulic fracturing. R Soc R Acad Eng 2012. http://www.raeng.org.uk/publications/reports/shale-gas-extraction-in-the-uk.

[8] Hajiyev A. A glimpse into ecological engineering based engineering management. Int J Manag Sci Eng Manag 2015;10(1):30–2. http://www.tandfonline.com/doi/pdf/10.1080/17509653.2014.974889?needAccess=true.

[9] Parliament UK. Environmental impact of development of shale gas in the UK (online). 2015. Accessed: 04.06.15, http://www.publications.parliament.uk/pa/ld201314/ldselect/ldeconaf/172/17210.htm.

[10] Cuadrilla Bowland Ltd. Lancashire shale gas exploration sites, Regulation 22 Information - Noise. 2015. http://www.lancashire.gov.uk/media/674854/LCC20140101-Noise-Report-Issue-to-LCC-4-3-15.pdf.

[11] Rootzén J, Johnsson F. CO2 emissions abatement in the Nordic carbon-intensive industry-An end-game in sight? Energy 2015;80:715–30. http://dx.doi.org/10.1016/j.energy.2014.12.029.

[12] Gavenas E, Rosendahl KE, Skjerpen T. $CO_2$-emissions from norwegian oil and gas extraction. Energy 2015;90:1956–66. http://dx.doi.org/10.1016/j.energy.2015.07.025.

[13] Heath GA, ODonoughue P, Arent DJ, Bazilian M. Harmonization of initial estimates of shale gas life cycle greenhouse gas emissions for electric power generation. Proc Natl Acad Sci 2014;111(31):E3167–76. http://www.pnas.org/content/111/31/E3167.full.pdf.

[14] Forster D, Perks J. Climate impact of potential shale gas production in the EU - final report (final report - review no. issue 2). AEA Technology Inc. for EC DG Climate Action; 2012. http://ec.europa.eu/clima/policies/eccp/docs/120815_final_report_en.pdf.

[15] MacKay DJ, Stone TJ. Potential greenhouse gas emissions associated with shale gas extraction and use. Department of Energy and Climate Change; 2013. https://www.gov.uk/government/uploads/system/uploads/attachment_data/file/237330/MacKay_Stone_shale_study_report_09092013.pdf.

[16] Bond CE, Roberts J, Hastings AFSJ, Shipton Z, Joao E, Tabyldy K, et al. SEPA - life-cycle assessment of greenhouse gas emissions from unconventional gas in Scotland, A ClimateXChange Scotland report. 2014. http://www.climatexchange.org.uk/reducing-emissions/life-cycle-assessment-ghg-emissions-unconventional-gas1/.

[17] New York State Department of Environmental Conservation. Well permit issuance for horizontal drilling and high-volume hydraulic fracturing to develop the Marcellus Shale and other low-permeability gas reservoirs. 2011. http://www.dec.ny.gov/data/dmn/rdsgeisfull0911.pdf.

[18] Adgate JL, Goldstein BD, McKenzie LM. Potential public health hazards, exposures and health effects from unconventional natural gas development. Environ Sci Technol 2014;48(15):8307–20. http://pubs.acs.org/doi/pdf/10.1021/es404621d.

[19] Rodriguez G. Air emissions characterization and management for natural gas hydraulic fracturing operations in the United States. Master's thesis. University of Michigan; 2013. https://deepblue.lib.umich.edu/handle/2027.42/97418.

[20] Sánta R, Garbai L, Fürstner I. Optimization of heat pump system. Energy 2015;89:45–54. http://dx.doi.org/10.1016/j.energy.2015.07.042.

[21] Warpinski N, Smith MB. Recent advances in hydraulic fracturing. SPE monograph series, vol. 12; 1989. ISBN:978-1-55563-020-1.

[22] EPA. Evaluation of impacts to underground sources of drinking water by hydraulic fracturing of coalbed methane reservoirs. Office of Ground Water and Drinking Water; 2004. EPA 816-R-04–003, http://large.stanford.edu/courses/2011/ph240/bogdanowicz2/docs/816-R-04-003.pdf.

[23] DECC, Andrews IJ. The Carboniferous Bowland Shale gas study: geology and resource estimation. British Geological Survey for Department of Energy and Climate Change; 2013. https://www.gov.uk/government/uploads/system/uploads/attachment_data/file/226874/BGS_DECC_BowlandShaleGasReport_MAIN_REPORT.pdf.

[24] Haimson B, Fairhurst C. Initiation and extension of hydraulic fractures in rocks. Soc Pet. Eng J 1967;7(03):310–8. https://www.onepetro.org/download/journal-paper/SPE-1710-PA?id=journal-paper%2FSPE-1710-PA.

[25] Hubbert MK, Willis DG. Mechanics of hydraulic fracturing, AAPG special volumes. 1972. http://www.depts.ttu.edu/gesc/Fac_pages/Yoshinobu/4361_5361_Folder/2013-readings/Hubbert%20and%20Willis%201972%20mechanics%20of%20hydr%20frac.pdf.

[26] Biot MA. Thermoelasticity and irreversible thermodynamics. J Appl Phys 1956;27(3):240–53. http://scitation.aip.org/content/aip/journal/jap/27/3/10.1063/1.1722351.

[27] Carcione JM, Cavallini F. Poisson's ratio at high pore pressure. Geophys Prospect 2002;50(1):97–106. http://www.researchgate.net/profile/Jose_Carcione2/publication/227731534_Poisson's_ratio_at_high_pore_pressure/links/00b4952dea37e54f91000000.pdf.

[28] American Petroleum Institute - API. Water management associated with hydraulic fracturing - HF2. 2010. http://www.shalegas.energy.gov/resources/HF2_e1.pdf.

[29] Gregory KB, Vidic RD, Dzombak DA. Water management challenges associated with the production of shale gas by hydraulic fracturing. Elements 2011;7(3):181–6. http://dx.doi.org/10.2113/gselements.7.3.181.

[30] Frac focus, what chemicals are used [online]. 2014. Accessed: 14.01.15, http://fracfocus.org/chemical-use/what-chemicals-are-used.

[31] Miller JE. The reciprocating pump: theory, design, and use. John Wiley & Sons; 1987. ISBN 0471854670, 9780471854678.

[32] American Petroleum Institute. 674 positive displacement, reciprocating, pumps, API standard. 1995.

[33] Fan T-g, Zhang G-q. Laboratory investigation of hydraulic fracture networks in formations with continuous orthogonal fractures. Energy 2014;74:164–73. http://dx.doi.org/10.1016/j.energy.2014.05.037.

[34] Karassik IJ, Krutzsch WC, Fraser WH, Messina JP. Pump handbook. 1986. ISBN: 9780080560052.

[35] Iannetti A, Stickland MT, Dempster WM. A computational fluid dynamics model to evaluate the inlet stroke performance of a positive displacement reciprocating plunger pump. Proc Inst Mech Eng Part A J Power Energy 2014. http://dx.doi.org/10.1177/0957650914530295.

[36] Meng H, Ludema K. Wear models and predictive equations: their form and content. Wear 1995;181:443–57. http://dx.doi.org/10.1016/0043-1648(95)90158-2.

[37] Josifovic A, Corney J, Davies B. Modeling a variable speed drive for positive displacement pump. In: Advanced intelligent mechatronics (AIM), IEEE/ASME international conference on, IEEE; 2014. p. 1218–23. http://dx.doi.org/10.1109/aim.2014.6878248.

[38] Hair JF, Tatham RL, Anderson RE, Black W. Multivariate data analysis. Pearson prentice hall upper Saddle River, NJ, vol. 6; 2006. ISBN: 978–0130329295.

[39] Saltelli A, Tarantola S, Campolongo F, Ratto M. Sensitivity analysis in practice: a guide to assessing scientific models. John Wiley & Sons; 2004.

[40] Experimental results - 1714311. Texas, USA: Fluid Lab; 2011.

[41] Zhang Y-J, Li Z-W, Guo L-L, Gao P, Jin X-P, Xu T-F. Electricity generation from enhanced geothermal systems by oilfield produced water circulating through reservoir stimulated by staged fracturing technology for horizontal wells: a

case study in Xujiaweizi area in Daqing Oilfield, China. Energy 2014;78:788–805. http://dx.doi.org/10.1016/j.energy.2014.10.073.
[42] StimPlan, Integrated 3d fracture design and analysis. NSI technologies; 2012. http://www.scandinasia.no.
[43] European Communities. Council directive 96/53/EC. Off J Euro Communities 1996. http://eur-lex.europa.eu/LexUriServ/LexUriServ.do?uri=OJ:L:1996:235:0059:0075:EN:PDF.
[44] NRG Manufacturing. 2500 HP frac pump unit, Tomball, Texas, USA. 2013. http://www.zycon.com/literature/1056616/2607888/nrgspec-4.0.1-frac-pump-2500-bhp.pdf.
[45] Worldsteel, Sustainability indicators (online). 2003. Accessed: 10.03.16, https://www.worldsteel.org/statistics/Sustainability-indicators.html.
[46] FIA, Formula one - power unit regulations. 2014. http://www.fia.com/sites/default/files/publication/file/FIA%20F1%20Power%20Unit%20leaflet.pdf.
[47] U.S. Energy Information Administration. Gasoline and diesel fuel update (online). 2016. Accessed: 10.03.16, https://www.eia.gov/petroleum/gasdiesel/.
[48] Xian H, Karali B, Colson G, Wetzstein ME. Diesel or compressed natural gas? A real options evaluation of the US natural gas boom on fuel choice for trucking fleets. Energy 2015;90:1342–8. http://dx.doi.org/10.1016/j.energy.2015.06.080.
[49] Engines for urban transit applications (online). Cummins Inc.; 2015. Accessed: 04.03.16, http://cumminsengines.com/brochure-download.aspx?brochureid=311.
[50] Caterpillar. Caterpillar natural gas engines (online). 2013. Accessed: 04.03.16, http://s7d2.scene7.com/is/content/Caterpillar/C10015265.
[51] Daneshy Consultants International. Hydraulic fracturing to improve production, Tech101. 2010. http://www.spe.org/twa/print/archives/2010/2010v6n3/09_Tech101.pdf.
[52] ICP. Well completion procedures in US, experimental field data. 2012.
[53] WeirSPM. TWS 2250HD well service pump, Fort Worth, Texas, USA. 2015. https://www.global.weir/assets/files/product%20brochures/SPM-Pump-Product-Catalog.pdf.

## Nomenclature

*Variables and constants*

$\sigma$: stress (Pa)
$r$: radius (m)
$\tau$: stress (Pa)
$\theta$: angle (rad)
$p$: pressure (Pa)
$\delta p$: pressure differential (Pa)
$T$: tensile strength (Pa)
$\beta$: poroelastic constant (-)
$\upsilon$: Poisson's ratio (-)
$\rho$: density ($kg/m^3$)
$H$: height (m)
$V$: volume ($m^3$)
$D$: diameter (m)
$MD$: measured depth (m)
$RL$: rod load (Nm)
$F$: force (N)
$R$: crank diameter (m)
$P$: power (W)
$Q$: flow rate (l/min)
$f$: frequency (Hz)
$n$: number of cylinders (-)
$a$: acceleration ($m/s^2$)
$v$: velocity (m/s)
$m$: mass (kg)
$s$: seconds
$X$: piston displacement (m)
$\alpha$: angle (rad)
$L$: con-rod length (m)
$t$: time (s)
$IN$: input
$A$: plunger area ($m^2$)
$\omega$: angular velocity (rad/s)
$rpm$: rotations per minute

*Subscripts and superscripts*

$rr$: radial direction
$\theta\theta$: tangential direction
$w$: wellbore
$x,y$: direction
$r\sigma$: shear direction
$b$: breakdown
$r$: pore
$H_{min}$: minimal horizontal
$H_{max}$: maximum horizontal
$V$: vertical
$i, j, k, l, o$: counters
$in$: intertia
$f$: friction
$sin$: single
$tot$: total
$n_1, n_2, n_3, n_4, n_5$: end counters